

1 Investigating the relationship between volume  
2 transport and sea surface height in a numerical  
3 ocean model

4 Estee Vermeulen <sup>1,2\*</sup>, Björn Backeberg <sup>2,3</sup>, Juliet Hermes <sup>1,4</sup>, Shane Elipot <sup>5</sup>

5 <sup>1</sup> *Department of Oceanography, University of Cape Town, Rondebosch, South Africa*

6 <sup>2</sup> *Nansen-Tutu Centre for Marine Environmental Research, Department of Oceanography,*  
7 *University of Cape Town, South Africa*

8 <sup>3</sup> *Nansen Environmental and Remote Sensing Center, Bergen, Norway*

9 <sup>4</sup> *South African Environmental Observation Network, Egagasini Node, Cape Town, South*  
10 *Africa*

11 <sup>5</sup> *Rosenstiel School of Marine and Atmospheric Science, University of Miami, 4600*  
12 *Rickenbacker Causeway, Miami, FL 33149*

13 *\*Corresponding author address: Estee Vermeulen, Department of Oceanography, University of*  
14 *Cape Town, Rondebosch, South Africa*

15 *Email: esteever01@gmail.com*

## 16 Abstract

17 The Agulhas Current Time-series mooring array (ACT) measured transport of the Agulhas  
18 Current at 34°S for a period of 3 years. Using along-track satellite altimetry data directly  
19 above the array, a proxy of Agulhas Current transport was developed based on the relationship  
20 between cross-current sea surface height (SSH) gradients and the measured transports. In  
21 this study, the robustness of the proxy is tested within a numerical modelling framework,  
22 using a 34-year long regional-hindcast simulation from the Hybrid Coordinate Ocean Model  
23 (HYCOM). The model specifically tested the sensitivity of the transport proxy to (1) changes  
24 in the vertical structure of the current and to (2) different sampling periods used to calculate the  
25 proxy. Two reference proxies were created using HYCOM data from 2010-2013, by extracting  
26 model data at the mooring positions and along the satellite altimeter track for; the box (net)  
27 transport and the jet (southwestward) transport. Sensitivity tests were performed where the  
28 proxy was recalculated from HYCOM for (1) a period where the modelled vertical stratification  
29 was different compared to the reference proxy, and (2) different lengths of time periods: 1, 3,  
30 6, 12, 18 and 34 years. Compared to the simulated (native) transports, it was found that  
31 the HYCOM proxy was more capable of estimating the box transport of the Agulhas Current  
32 compared to the jet transport. This was because the model is unable to resolve the dynamics  
33 associated with meander events, for which the jet transport algorithm was developed. The  
34 HYCOM configuration in this study contained exaggerated levels of offshore variability in the  
35 form of frequently-impinging baroclinic anticyclonic eddies. These eddies consequently broke  
36 down the linear relationship between SSH slope and vertically-integrated transport. Lastly,  
37 results showed that calculating the proxy over shorter or longer time periods in the model  
38 did not significantly impact the skill of the Agulhas transport proxy. Modelling studies of  
39 this kind provide useful information towards advancing our understanding of the sensitivities  
40 and limitations of transport proxies that are needed to improve long-term ocean monitoring  
41 approaches.

## 1 Introduction

The Agulhas Current System is the strongest western boundary current in the Southern Hemisphere and transports warm tropical water southward along the east coast of South Africa [Lutjeharms, 2006]. The Agulhas Current, in the northern region, is known for its narrow, fast, flow conditions following the steep continental slope [de Ruijter et al., 1999]. As the current continues southwestward it becomes increasingly unstable over the widening continental shelf until it eventually retroflects, forming an anticyclonic loop south of Africa and returning to the Indian Ocean as the eastward Agulhas Return Current [Beal et al., 2011; Biastoch and Krauss, 1999; Dijkstra and de Ruijter, 2001; Hermes et al., 2007; Lutjeharms, 2006; Loveday et al., 2014]. The anticyclonic loop, known as the Agulhas Retroflection, contains some of the highest levels of mesoscale variability in the global ocean [Gordon, 2003] in the form of Agulhas rings, eddies and filaments. These contribute heat, salt and energy into the Benguela upwelling system, the Atlantic Ocean and the global overturning circulation system [Gordon et al., 1987; Beal et al., 2011; Durgadoo et al., 2013], impacting the Atlantic Meridional Overturning Circulation (AMOC) [Biastoch and Krauss, 1999; Beal et al., 2011; Durgadoo et al., 2013; Loveday et al., 2014]. In the regional context, the Agulhas Current has a major influence on the local weather systems, due to large latent and sensible heat fluxes, which contributes to rainfall and storm events over the adjacent land [Reason, 2001; Rouault et al., 2002; Rouault and Lutjeharms, 2003]. The unique circulation of the Agulhas Current System, in the context of regional and global climate variability, makes it an important field of research.

To understand the complicated dynamics of the Agulhas Current requires an integrated approach using numerical ocean models, satellite remote sensing measurements and *in situ* observations. Previous studies have suggested that measuring the dynamics of the Agulhas Current in the northern region is easier due to its stable trajectory and its confinement to the continental slope [van Sebille et al., 2010]. However, the close proximity of the current to the coast has made it difficult to monitor using satellite altimetry [Rouault et al., 2010]. Newer altimetry products dedicated to coastal areas are promising but are yet to be validated within the Agulhas Current region [Birol et al., 2017]. In addition,

72 the frequent disturbances of the current in the form of solitary meanders, also known as  
73 Natal Pulses, and its interactions with mesoscale features originating upstream and from  
74 the east [Elipot and Beal, 2015], remain poorly resolved in many numerical ocean models  
75 [Tsugawa and Hasumi, 2010; Braby et al., 2016], highlighting the challenges involved in  
76 monitoring and modelling the dynamics in this region.

77 There is a trade-off between spatial and temporal sampling. *In situ* mooring observa-  
78 tions provide high temporal observations of the Agulhas Current throughout the water  
79 column but are spatially coarse. In contrast, satellite observations can provide high spa-  
80 tial resolution data of the surface ocean but lacks detailed information below the surface.  
81 Hence, numerical models are needed to provide a temporally coherent, high resolution  
82 representation of the ocean throughout the water column. Numerous studies aiming to  
83 monitor long-term changes in global current systems have adopted methods to combine  
84 various sampling tools [eg. Maul et al. 1990; Imawaki et al. 2001; Andres et al. 2008; Zhu  
85 et al. 2004; Yan and Sun 2015], including the recent development of the Agulhas transport  
86 proxy established to monitor the interannual variability and long-term trends in Agulhas  
87 Current transport [Beal and Elipot, 2016].

88 Beal and Elipot [2016] have shown that a strong relationship exists between surface geo-  
89 strophic velocity and full-depth transport such that sea level anomalies can be used to  
90 study the variability and dynamics of the Agulhas Current System as has been demon-  
91 strated before [Fu et al., 2010; Rouault et al., 2010; Rouault and Penven, 2011; etc.].  
92 The 22-year transport proxy created by Beal and Elipot [2016] assumed a fixed linear  
93 relationship between *in situ* transport and sea surface slope based on *in situ* measure-  
94 ments over the 3-year sampling period of the Agulhas Current Time-series experiment  
95 (ACT) [Beal et al., 2015]. Analyses of the Agulhas Current transport proxy time-series  
96 concluded that the Agulhas Current has not intensified over the last two decades in re-  
97 sponse to intensified global winds under anthropogenic climate change [Cai, 2006; Yang  
98 et al., 2016], but instead has broadened as a result of increased eddy activity [Beal and  
99 Elipot, 2016] in agreement with Backeberg et al. [2012]. This could essentially decrease  
100 poleward heat transport and increase mixing over the continental shelf, thereby increasing  
101 cross-frontal exchange of nutrients and pollutants between the coastal ocean and the deep  
102 ocean [Backeberg et al., 2012; Beal and Elipot, 2016].

103 This modelling study recreates the Agulhas transport proxy developed by Beal and Elipot  
104 [2016], within a regional HYCOM simulation of the greater Agulhas Current System,  
105 aiming to test the sensitivity of using 3 years of *in situ* mooring data to develop a transport  
106 proxy as well as the sensitivity of the proxy to changes in the vertical structure of the  
107 Agulhas Current. The paper is structured as follows; Section 2 describes the data and  
108 methods, it should be noted that this section forms a key part of the paper as the methods  
109 of recreating the proxy are an integral component of the study. Section 3 presents the  
110 results from the HYCOM transport proxy and lastly Section 4 presents the summary and  
111 conclusions.

## 112 **2 Data and Methods**

### 113 **2.1 The Hybrid Coordinate Ocean Model**

114 The Hybrid Coordinate Ocean Model (HYCOM) is a primitive equation ocean model  
115 that was developed from the Miami Isopycnic Coordinate Ocean Model (MICOM) [Smith  
116 et al., 1990]. HYCOM combines the optimal features of isopycnic-coordinate and fixed-  
117 grid ocean circulation models into one framework [Bleck, 2002] and uses the hybrid layers  
118 to change the vertical coordinates depending on the stratification of the water column.  
119 The model makes a dynamically smooth transition between the vertical coordinate types  
120 via the continuity equation using the hybrid coordinate generator [Chassignet et al., 2007].  
121 Well-mixed surface layers use z-level coordinates,  $\rho$ -coordinates are utilized between the  
122 surface and bottom layers in a well-stratified ocean, and the bottom layers apply  $\sigma$ -  
123 coordinates following bottom topography. Adjusting the vertical spacing between the  
124 hybrid coordinate layers in HYCOM simplifies the numerical implementation of several  
125 physical processes without affecting the efficient vertical resolution, and thus combines  
126 the advantages of the different coordinate types in optimally simulating coastal and open-  
127 ocean circulation features [Chassignet et al., 2007].

128 This study used output from a one-way nested  $1/10^\circ$  model of the greater Agulhas Current  
129 System (AGULHAS) [Backeberg et al., 2008; 2009; 2014]. The regional nested model,  
130 AGULHAS, received boundary conditions from the basin-scale model of the Indian and  
131 Southern Ocean (INDIA) [George et al., 2010] every 6-hrs. The boundary conditions

132 were relaxed towards the outer model over a 20 grid cell sponge layer. The nested model  
133 covered the region from the Mozambique Channel to the Agulhas Retroflexion region  
134 and the Agulhas Return Current, geographically extending from approximately 0°-60°  
135 East and from 10°-50° South, with a horizontal resolution of  $\sim 10$  km that adequately  
136 resolved mesoscale dynamics to the order of the first baroclinic Rossby radius estimated  
137 to be about 30 km [Chelton et al., 1998]. AGULHAS has 30 hybrid layers and targeted  
138 densities ranging from 23.6 to 27.6 kg/m<sup>3</sup>.

139 AGULHAS was initialised from a balanced field of the parent model interpolated to the  
140 high-resolution grid and ran from 1980 to 2014 using interannual forcing from ERA40  
141 [Uppala et al., 2005] and ERA-interim [Dee et al., 2011]. Version 2.2 of the HYCOM source  
142 code has been used in this model and, together with the second order advection scheme,  
143 provides an adequate representation of the Agulhas Current [Backeberg et al., 2014].  
144 However, limitations of the free running model include high levels of SSH variability south  
145 of Madagascar and offshore of the Agulhas Current, suggesting that eddy trajectories may  
146 be too regular in the model [Backeberg et al., 2014]. The data available for this study  
147 was a weekly output of the regional HYCOM model of the Agulhas region from 1980 to  
148 2014.

## 149 **2.2 The Agulhas Current Time-series Experiment**

150 The ACT experiment was established to obtain a multi-decadal proxy of Agulhas Current  
151 transport using satellite altimeter data. The first phase of the experiment was the *in situ*  
152 phase where the ACT mooring array was deployed in the Agulhas Current, near 34°S,  
153 for a period of three years from: 2010-2013 [Beal et al., 2015] (Figure 1). From the  
154 data collected, Beal et al. [2015], provided two volume transport estimates: (1) a box or  
155 boundary layer transport ( $T_{box}$ ) and (2) a western boundary jet transport ( $T_{jet}$ ).  $T_{box}$  is  
156 the net transport within a fixed distance from the coast, while  $T_{jet}$  is a stream dependent  
157 transport that is calculated by changing the boundaries of integration at each time step  
158 depending on the strength and cross-sectional area of the southwestward jet. The western  
159 boundary jet transport algorithm was developed to specifically exclude the northeastward  
160 transport during meander events, occurring inshore of the meander [Beal et al., 2015].

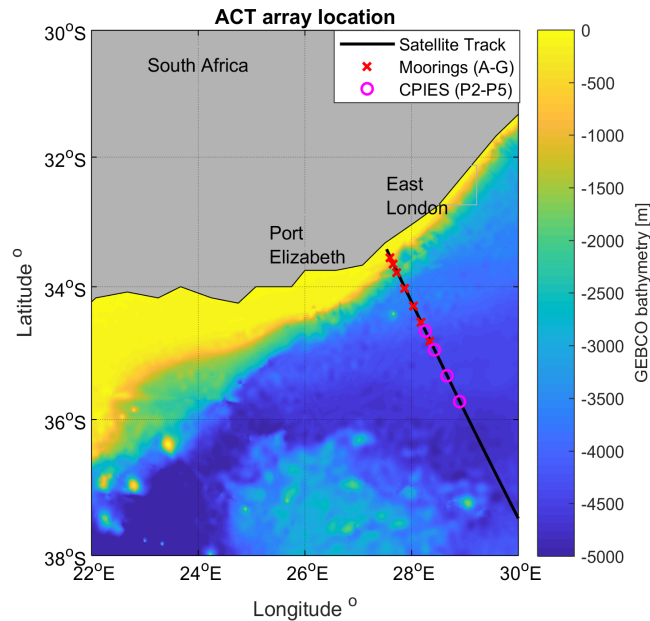


Figure 1: Geographical location of the ACT array with the mooring (red crosses) and CPIES (magenta circles) stations relative to the T/P, Jason-1,2,3 satellite track #96 (black line). Colour shading illustrates the GEBCO bathymetry (m).

161 During the second phase of the ACT experiment, Beal and Elipot [2016] built a 22-year  
 162 transport proxy by regressing the three years of *in situ* transport measurements (obtained  
 163 from phase 1) against along-track satellite altimeter data spanning the years 1993-2015.

### 164 2.3 Development of the Agulhas transport proxy

165 Previous analyses have shown that the vertical structure of the Agulhas Current is baro-  
 166 tropic [Elipot and Beal, 2015], implying that the relationship between surface geostrophic  
 167 velocity and full depth transport should be strong, despite the presence of the Agulhas  
 168 Undercurrent [Beal and Elipot, 2016] (Figure 2). Access to the data from the ACT ex-  
 169 periment allowed us validate the velocity cross-section in HYCOM (Figure 2). Beal et al.  
 170 [2015] defined the Agulhas Current to be 219 km wide and 3000 m deep on average, as is  
 171 reflected in the vertical section of the *in situ* ACT observations (Figure 2a). In HYCOM  
 172 the current is wider, weaker and further offshore than the observed current, on average  
 173 the current is 254 km wide and extends deeper down to  $\sim 3500$  m, particularly inshore,  
 174 with a less pronounced undercurrent (Figure 2b).

175 The transport proxy created by Beal and Elipot [2016] was initially developed by finding  
 176 a linear relationship between transport and sea surface slope across the entire length

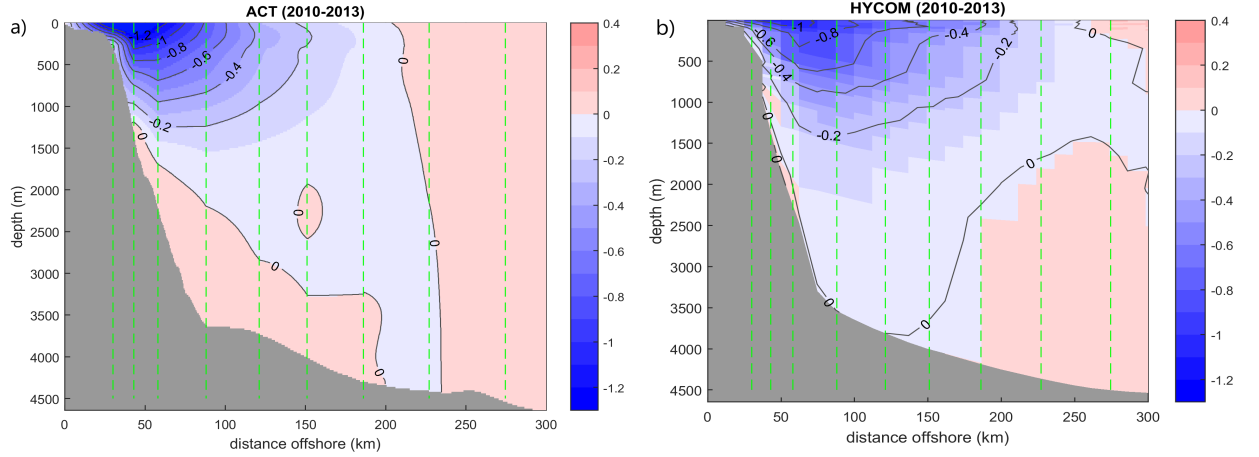


Figure 2: Time mean cross-section of the velocity structure of the Agulhas Current across the ACT array ( $ms^{-1}$ ) during the *in situ* ACT period (2010-2013) from (a) the ACT Observations (b) the HYCOM-AGULHAS simulation. Blue shading represents the negative, southwest current direction and pink shading represents the positive, northeast current flow. Contours are every  $0.2 ms^{-1}$ . Dashed green vertical lines represents the nine locations of the mooring and CRIES-pairs, the first line representing mooring A and CRIES-pair P4P5 furthest offshore.

177 of the ACT array, a common method used in previous studies [Imawaki et al., 2001;  
 178 van Sebille et al., 2010; Sprintall and Revelard, 2014; Yan and Sun, 2015]. However,  
 179 this method lead to uncertainty in the linear regression due to the strong, co-varying  
 180 sea surface height across the current. The preferred method was therefore to build nine  
 181 individual linear regression models, one for each mooring position and CRIES-pairs along  
 182 the ACT array, which locally related transport to sea surface slope [Beal and Elipot,  
 183 2016]. It is important to note that the regression models assumed a constant, linear  
 184 relationship between sea surface slope and transport over the three-year *in situ* period.  
 185 The transport variable in the regression models was defined as transport per unit distance,  
 186 i.e. the vertically integrated velocity with units in  $m^2s^{-1}$ , where  $T_x$  represents the net  
 187 component of the current flow and  $T_{xsw}$  the southwestward component of the flow. The  
 188 total transports,  $T_{box}$  and  $T_{jet}$  in  $m^3s^{-1}$ , were calculated by integrating the  $T_x$  and  $T_{xsw}$   
 189 estimates, predicted from the regression models, to the respective current boundaries.

#### 190 2.4 Recreating the Agulhas transport proxy in HYCOM

191 In order to recreate the Agulhas Current proxy in HYCOM, data corresponding to the  
 192 measurements collected from the ACT mooring array were extracted from the model. To  
 193 build the regression models the transport per unit distance and sea surface slope for each  
 194 of the nine mooring locations were calculated using the model data (hereafter CRIES



195 pairs P3-P4 and P4-P5 were included as mooring positions 8 and 9).

#### 196 **2.4.1 Model Transport**

197 The barotropic velocity -equivalent to an integral of the velocity with depth- from each  
198 mooring location (A-G) and CPIES pairs P3-P4 and P4-P5 [Beal et al., 2015] was ex-  
199 tracted for the 34-year model period. Extracting the barotropic velocity component from  
200 each mooring avoided interpolation errors that may have occurred if the model velocity  
201 was interpolated onto the locations of each current-meter instrument on each mooring  
202 [e.g. van Sebille et al., 2010]. Transport per unit distance ( $Tx$ ) for each mooring was cal-  
203 culated by multiplying the cross-track barotropic velocity by the respective depth at each  
204 mooring location. The same method was employed to calculate the southwest transport  
205 component ( $Txsw$ ) excluding the northeast cross-track barotropic velocity values in the  
206 calculation.

#### 207 **2.4.2 Model SSH**

208 In order to reproduce the “along-track” SSH altimeter data needed to create the proxy as  
209 in Beal and Elipot [2016], 34 years of HYCOM SSH was linearly interpolated onto the  
210 coordinates of the TOPEX/Jason satellite track number 96 overlapping the model ACT  
211 array. The coordinates of the along-track altimeter data were obtained from the filtered  
212 12 km Jason-2 Aviso satellite product. To obtain the sea surface slope for each regression  
213 model, an optimal pair of SSH data points was chosen such that the horizontal length  
214 scale between them allowed for a maximum correlation between sea surface slope and  $Tx$ .  
215 The length scales of the slopes ranged from 24 km at mooring A to 12 km at mooring  
216 G and 48 km for the offshore CPIES-pairs, indicating an increase in the spatial scale  
217 of offshore flow, possibly due to increased offshore variability. Results from the *in situ*  
218 proxy experiment by Beal and Elipot [2016] also showed an increasing length scale with  
219 increasing distance offshore, however the results varied in magnitude: 27 km at mooring B  
220 to 102 km at mooring G. In this study the SSH slope was calculated such that a negative  
221 SSH slope corresponds to a negative surface velocity (southwest) according to geostrophy,  
222 whereas a positive slope would indicate positive northeastward flow.

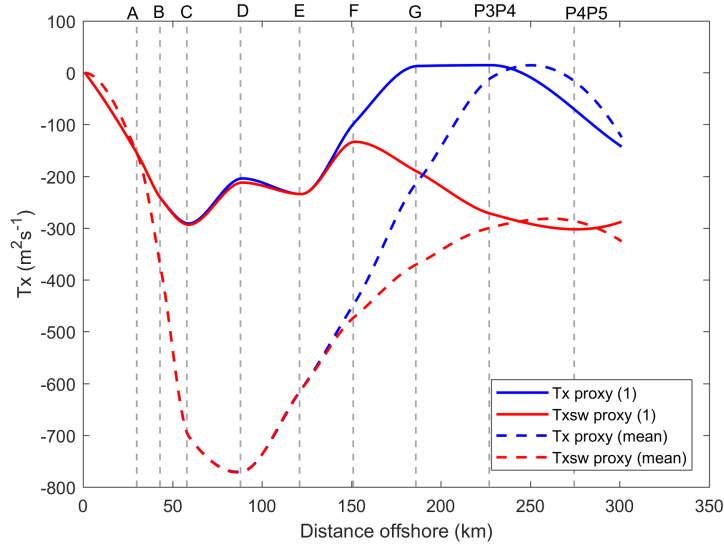


Figure 3: HYCOM transport per unit distance proxy ( $\text{m}^2 \text{s}^{-1}$ ) for  $T_x$  (blue) and  $T_{xsw}$  (red) at 1 km intervals at the first model time step (solid lines) and for the ACT reference period (2010-2013, dashed lines). The grey dashed-lines represent the positions of moorings and offshore CPIES pairs.

### 2.4.3 Building the regression models

Nine linear regression models were developed to estimate the transport per unit distance ( $T_x$  and  $T_{xsw}$ ) from the HYCOM sea surface slope during the same three-year period over which the ACT proxy was developed (April 2010- February 2013). The three-year time period is hitherto referred to as the reference period.

To calculate the total transport across the ACT array required continuous  $T_x$  estimates across the current. This was achieved as in Beal and Elipot [2016] by fitting a piecewise cubic Hermite interpolating polynomial function to obtain transport estimates at 1 km intervals from the coast to the end of the array (Figure 3). Fitting the transport function to the coast and equating it to zero would be equivalent to implementing a no slip boundary condition in the model. Before calculating the total transport the current boundaries needed to be defined. The box transport ( $T_{\text{box}}$ ) was calculated by integrating  $T_x$  horizontally to 230 km offshore, the three-year mean width of the current in HYCOM. The jet transport ( $T_{\text{jet}}$ ) was calculated using the algorithm developed by Beal et al. [2015] by integrating  $T_{xsw}$ , the southwest transport component, to the first maximum of  $T_x$  beyond the half-width of the current (115 km in HYCOM) at each time step (Figure 3).

239 Assuming that the three-year linear relationship between SSH slope and transport per  
240 unit distance ( $T_x$  and  $T_{xsw}$ ) from 2010-2013 remains constant, the regression models  
241 were applied to the entire 34-year SSH model data. Thereafter, the 34-year transports  
242 were calculated by applying the same methods that were used to calculate the 3-year  
243 transport time-series; firstly, obtaining  $T_x$  and  $T_{xsw}$  estimates at 1 km-intervals along  
244 the array and secondly integrating horizontally to obtain  $T_{box}$  and  $T_{jet}$ .

## 245 **2.5 Comparison of the transport proxy to actual model transports**

246 The simulated model transports were calculated using the full-depth velocity fields across  
247 the array. If the relationship between SSH slope and transport is strong, there would be  
248 good agreement between the proxy and the actual model transports. To quantify this,  
249 correlations and transport statistics for the model and proxy were calculated from the two  
250 time-series (Table 2). These provided insight into which processes the proxy may have  
251 failed to capture, which were then further investigated in HYCOM. Statistics are deemed  
252 significant at the 95% significance level.

253 Eddy kinetic energy (EKE) was calculated to show the surface variability of the current  
254 coincident with averaged SSH contours used to represent the mean surface structure  
255 (Figure 6). EKE was calculated over the 3-year mean reference period, and over the  
256 highest and lowest correlated years. In order to evaluate the subsurface current structure  
257 along the ACT array, vertical velocity profiles were analysed for each mooring and CPIES-  
258 pair over the 3-year mean reference period as well as over the highest and lowest correlated  
259 years.

260 Transport variability in HYCOM was analysed by investigating the current structure  
261 during the residual transport events in the least and best performing regression models.  
262 Residual transport events were identified as the outlying residual transport values above  
263 and below 2 standard deviations of the estimated transport.

$$e = Txi - \hat{Txi} \quad (1)$$

264 where  $e$  is the estimated residuals,  $Txi$  is the HYCOM transport per unit distance value  
265 and  $\hat{Txi}$  is the estimated transport per unit distance value according to the linear regres-

266 sion models (i.e the transport proxy).

267 To investigate the current structure during these residual events, composite averages of  
268 the cross-track velocity structure were analysed. The cross-track velocity at each depth  
269 layer in HYCOM was extracted at 12 km intervals from 0 km to 400 km offshore, for the  
270 34-year model period. Although the ACT array only reached 300 km offshore, analysis of  
271 the current structure in HYCOM was extended further offshore. Previous analyses have  
272 shown increased levels of offshore variability in this HYCOM simulation [Backeberg et al.,  
273 2009; 2014], which therefore made it interesting to study the subsurface structure during  
274 the offshore current meanders and the influence these could have on the transport proxy.  
275 To further investigate the effect of the residual transport values on the transport proxy,  
276 all corresponding transport events exceeding plus or minus two standard deviations were  
277 removed from each linear regression model during development of the proxy (Figure 4).

## 278 **2.6 Sensitivity tests**

279 Sensitivity experiments were performed in HYCOM to test how many years of mooring  
280 data is needed to create an accurate proxy of Agulhas Current transport. With 34 years  
281 of model data the linear relationship could be tested over much longer or shorter periods.  
282 Using the method described in section 2.4.3, the proxy regression models were built using  
283 1, 6, 12, 18 and 34 years of HYCOM data. In addition, the proxies were calculated over  
284 two arbitrary 3-year periods, to test the sensitivity of the proxy to current dynamics  
285 over different years. Lastly, the regression models were calculated over the maximum and  
286 minimum annual transport years in HYCOM, as well as during the years the HYCOM  
287 transport standard deviation was the largest and the smallest. Table 1 shows the time  
288 range over which the sensitivity experiments were performed.

Table 1: Sensitivity experiment time periods.

Time range (years)	Model dates
1	Jan 2011 - Dec 2011
3	Apr 2010 - Feb 2013
6	Jan 2009 - Dec 2014
12	Jan 2003 - Dec 2014
18	Jan 1997 - Dec 2014
34	Jan 1980 - Dec 2014
3*	Jan 1980 - Dec 1982; Jan 2000 - Dec 2002
Max (Min) HYCOM transport.	2003 (1982)
Max (Min) HYCOM transport STD.	2013 (1980)

3\* Corresponds to the two additional 3-year periods

## 289 3 Results

### 290 3.1 HYCOM linear regression models

291 The coefficient of determination ( $R^2$ ) from the regression models highlight how well the  
292 linear relationship predicts the transport in HYCOM (Figure 4).  $R^2$  ranged from 0.86 at  
293 mooring A (30 km offshore) to 0.49 at the last CPIES-pair P4P5 (275 km offshore) for  
294  $T_x$  and 0.86 at mooring A to 0.37 at P4P5 for  $T_{xsw}$  (P values  $< 10^{-3}$ ). Results from Beal  
295 and Elipot [2016] showed an increase in the  $R^2$  statistics in the regression models ranging  
296 from 0.51 at mooring A and 0.81 for CPIES-pair P4P5 for  $T_x$ , indicating that the *in situ*  
297 observation based regression models had poorer skill inshore, whereas in HYCOM the  
298 regression models have poorer skill offshore. The results from the  $T_{xsw}$  regression models  
299 in HYCOM showed similar results to Beal and Elipot [2016] for the inshore mooring  
300 locations (A, B, C, E) with slightly higher correlations for offshore moorings F, G and  
301 CPIES-pair P3P4 but a lower correlation for D and the furthest CPIES-pair P4P5.

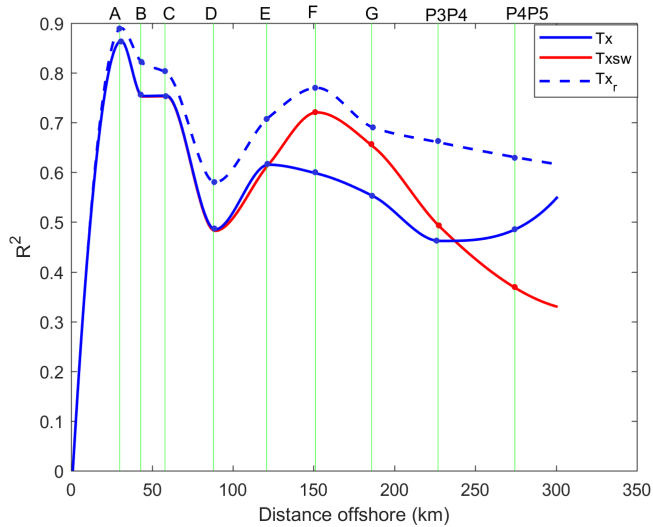


Figure 4:  $R^2$  statistics from the linear regression models showing the relationship between HYCOM SSH slope and HYCOM transport per unit distance for each mooring (A-G) and CRIES-pair (P3P4 & P4P5) over the 3-year reference period (2010-2013).  $T_x$  is represented by the solid blue line and  $T_{xsw}$  by the solid red line. The dashed blue line represents the results of  $T_x$  after the removal of the residual transport events (see section 3.4). Sites A - CRIES pair P4P5 are shown by the faint green lines.

### 302 3.2 Proxy validation

303 Two transport types, the box transport ( $T_{box}$ ) and the jet transport ( $T_{jet}$ ) were extracted  
 304 from HYCOM in order to validate the relative proxies. The  $T_{box}$  ( $T_{jet}$ ) proxy explained  
 305 57% (14%) of transport variance during the three-year reference period (2010-2013) (Table  
 306 2b). Using 34-years of model data (1980-2014), assuming the fixed 3-year relationship  
 307 between SSH slope and transport,  $T_{box}$  ( $T_{jet}$ ) explained 52% (26%) of the transport  
 308 variance (Table 2b). Results from Beal and Elipot [2016] also showed that  $T_{box}$  explained  
 309 a higher percentage of variance (61%) during the ACT period than the jet transport proxy  
 310 ( $T_{jet}$ : 55%).

311 The 34-year mean transport and standard deviation from HYCOM for  $T_{box}$  and  $T_{jet}$  was  
 312  $-84 \pm 47$  Sv and  $-110 \pm 38$  Sv respectively (Table 2a). The proxy  $T_{box}$  and  $T_{jet}$  was  $-87$   
 313  $\pm 34$  Sv and  $-92 \pm 31$  Sv respectively (Table 2a). According to the ACT observations  
 314 the mean transport and standard deviation was  $-77 \pm 32$  Sv for  $T_{box}$  and  $-84 \pm 24$  Sv for  
 315  $T_{jet}$ . A higher jet transport was expected considering it excludes northeast counter-flows  
 316 that decrease the box transport [Beal et al., 2015]. The differences between the standard  
 317 deviations of HYCOM and the proxy indicate that transport in HYCOM experiences more

Table 2: a) Summary of the transport statistics of the ACT observations over the 3-year *in situ* period and the HYCOM model transports and HYCOM proxy transports over the 3-year and extended 34-year time period. Negative values denote transport in the southwest direction.  $1 \text{ Sv} = 10^6 \text{ m}^3 \text{ s}^{-1}$ . b) Correlations between the HYCOM model transport and HYCOM proxy transport, for the box transport and jet transport with the percentage of variance shown in brackets. All correlations were significant.

a)	ACT (2010-2013)		HYCOM (2010-2013)		Proxy		HYCOM (1980-2014)		Proxy	
Transport	$T_{box}$	$T_{jet}$	$T_{box}$	$T_{jet}$	$T_{box}$	$T_{jet}$	$T_{box}$	$T_{jet}$	$T_{box}$	$T_{jet}$
Mean & Std (Sv)	$-77 \pm 32$	$-84 \pm 24$	$-81 \pm 53$	$-112 \pm 41$	$-91 \pm 35$	$-92 \pm 30$	$-84 \pm 47$	$-110 \pm 38$	$-87 \pm 34$	$-92 \pm 32$
Max (Sv)	-157	-174	-223	-244	-196	-185	-236	-245	-213	-219
Min (Sv)	23	-25	44	-48	-36	-46	87	-30	-20	-27

b)	$T_{box}$	$T_{jet}$
2010-2013	0.75 (57%)	0.38 (14%)
1980-2014	0.72 (52%)	0.51 (26%)

318 variability compared to the proxy. The proxies only capture a portion of the transport  
319 estimate from HYCOM, suggesting it also only captures a portion of the model variability.  
320 The positive minimum transport values for  $T_{box}$  during both time periods also appear to  
321 be peculiar, suggesting a current reversal during those events (Table 2a).

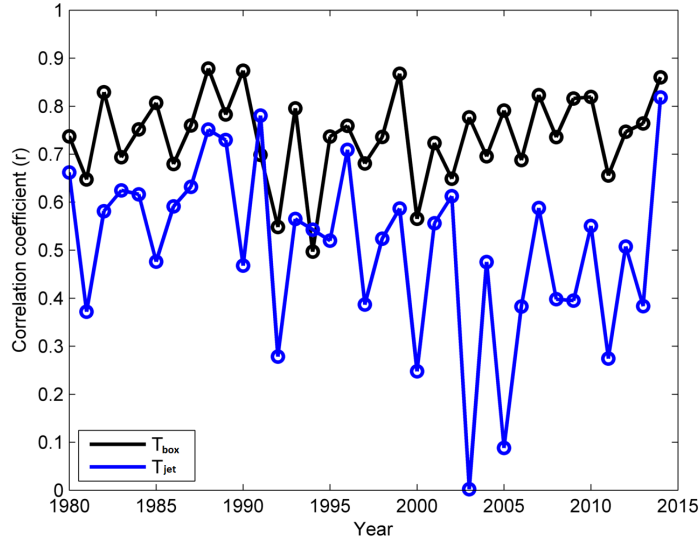


Figure 5: 34-year annual correlations between the box (black) and jet (blue) transport proxies against the box and jet transports extracted from HYCOM.

322 The  $T_{jet}$  annual correlation varies greatly from year to year with a significant maximum  
323 correlation of 0.82 (2014) and a minimum correlation of 0.00 (2003) (Figure 5). In con-

324 trast, the correlations for  $T_{box}$  vary much less and are always significant with a maximum  
325 correlation of 0.88 (1988) and minimum correlation of 0.50 (1994) (Figure 5). The box  
326 transport has higher correlations for most of the 34-year time period except during two  
327 single years where the jet transport has a higher correlation, 0.78 versus 0.70 during 1991  
328 and 0.54 versus 0.50 during 1994. These results indicate that the proxy is generally better  
329 suited in HYCOM to estimate the box transport rather than the jet transport.

330 The jet transport proxy by Beal and Elipot [2016] was developed to estimate the transport  
331 of the Agulhas Current during mesoscale meander events, which generally causes the  
332 current to manifest as a full-depth, surface intensified, cyclonic circulation out to 150 km  
333 from the coast with anticyclonic circulation farther offshore [Elipot and Beal, 2015]. The  
334 Agulhas meanders in the HYCOM simulation occur in association with large anticyclonic  
335 eddies predominantly located at the offshore edge of the current, with a narrow, southwest  
336 stream close to the coast [Backeberg et al., 2009]. In some instances anticyclonic eddies  
337 span the length of the entire array. Therefore, considering that the model is unable to  
338 resolve the dynamics associated with meander events, for which the jet transport algorithm  
339 was specifically developed, further analysis only focuses on the box transport proxy.

### 340 **3.3 Evaluating the box transport proxy**

341 The strengths and weaknesses of the box proxy are further investigated by selecting the  
342 highest and lowest correlated years from the 34-year annual correlations (Figure 5), and  
343 evaluated by plotting the current structure in the model over the respective years (Figures  
344 6 & 7).

345 During the year with maximum correlation (1988) the current is stable and inshore,  
346 whereas during the lowest correlated year (1994) and during the proxy reference period  
347 (2010-2013) the current is meandering and it appears that a large portion of the energy  
348 of the current has been shifted offshore (Figure 6). The narrow spacing of the SSH  
349 contours for all three periods indicates a strong gradient inshore and hence a strong  
350 mean geostrophic current, however the wide spacing between the SSH contours offshore  
351 suggests that the variability in the model is confined to the offshore side of the current.  
352 It is assumed that high levels of mesoscale variability in the model could bias the current  
353 position and hence the transport estimate. However, based on the analysis there were  $\sim 5$



354 anticyclonic eddies during the highest correlated year (1988) and  $\sim 7$  anticyclonic eddies  
355 during the lowest correlated year (1994) which does not explain the difference in the  
356 accuracy of the proxy for those years.

357 The model cross-track velocity changes direction with depth, specifically for offshore moor-  
358 ing G and CPIES-pairs P3P4 and P4P5, at the depth of  $\sim 2000$  m (Figure 7) thereby  
359 defining the depth of the Agulhas jet. During the 3-year reference period the velocity  
360 changes direction at moorings B and G ( $\sim 1200$  m and  $\sim 2000$  m respectively) and at  
361 sites P3P4 ( $\sim 2000$  m) and P4P5 ( $\sim 300$  m,  $\sim 2000$  m). During 1988, sites F-P4P5 exper-  
362 ience a change in direction ( $> \sim 2000$  m). Lastly, during 1994 mooring G and sites P3P4  
363 and P4P5 exhibit a change in direction ( $> \sim 2000$  m). An explanation for the offshore  
364 subsurface countercurrents may be due to the impinging baroclinic eddies continuously  
365 propagating downstream [Backeberg et al., 2009], affecting the entire water column by  
366 changing the direction of flow at certain depths. This directly impacts the accuracy of the  
367 proxy and explains why the transport proxy fails to capture current reversals (Table 2),  
368 because the SSH slope does not capture the subsurface countercurrents associated with  
369 the impinging baroclinic eddies.

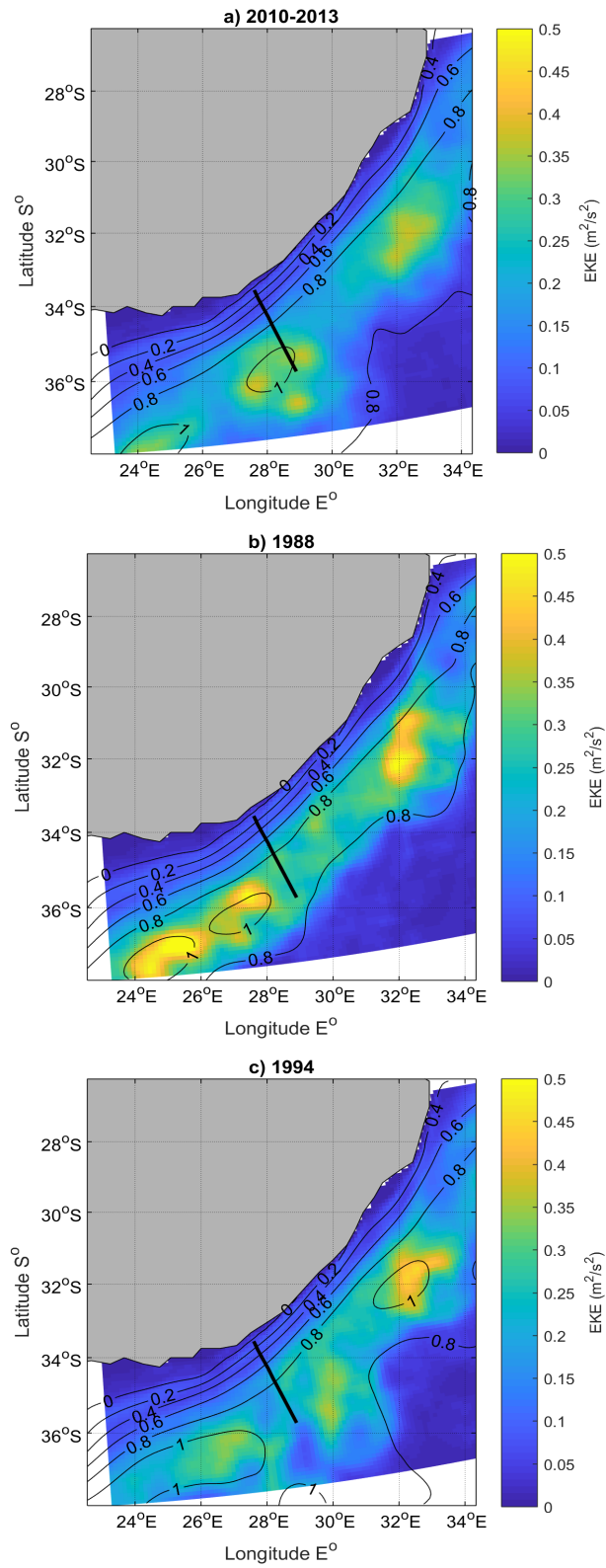


Figure 6: Eddy kinetic energy (EKE in  $\text{m}^2\text{s}^{-2}$ ) and sea surface height (SSH in m) contours during (a) the reference period (2010-2013) (b) the highest (1988) and (c) lowest (1994) correlated years. The black line representing the ACT array.

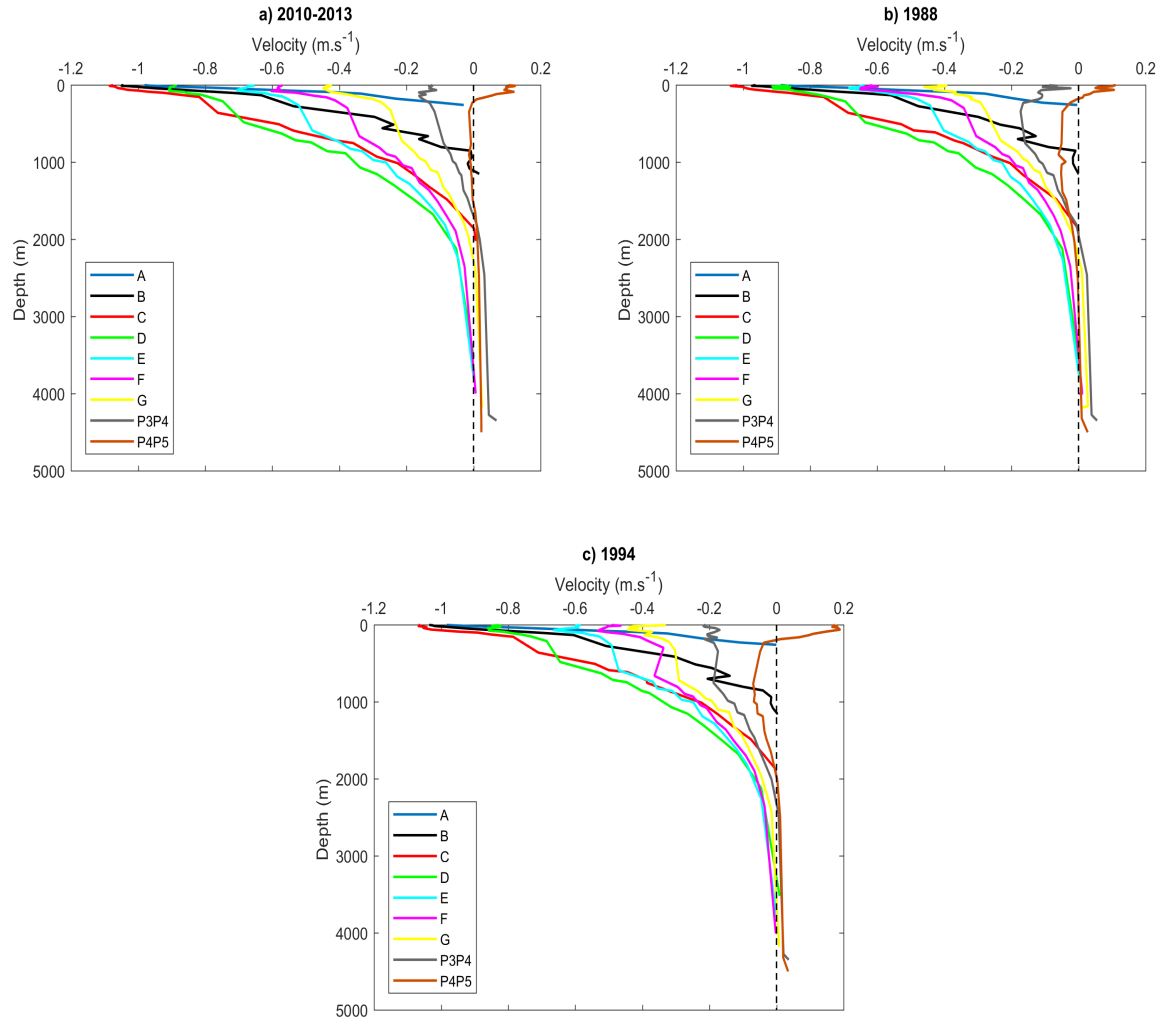


Figure 7: Mean cross-track velocity profiles ( $\text{m s}^{-1}$ ) during (a) the 3-year reference period (2010-2013), (b) during the highest correlated year (1988) and (c) the lowest correlated year (1994). Each colour represents the different moorings (A-G) and CPIES-pairs (P3P4 & P4P5). Negative values indicate southwestward flow.

### 370 3.4 Investigating the transport variability

371 As shown previously, the performance of the linear regression models weakened moving  
 372 offshore (Figure 4). Regression model, RM8 (CPIES-pair P3P4, Figure 8a) captured the  
 373 least transport variance at 46% and RM 1 (mooring A, Figure 8b) explained the most  
 374 transport variance at 86%. According to our methods, a negative SSH slope in HYCOM  
 375 corresponds to a negative (southwest) surface velocity and if the current structure were  
 376 barotropic, a negative (southwest) transport and vice versa.

377 As shown in RM 1 (Figure 8b), all the data points are clustered such that the negative SSH  
 378 slope relates to a negative  $T_x$  value, in the absence of northeast counterflows. Careful

379 analyses of RM 8 indicates that eight of the nine residual transport events violate the  
 380 proportional relationship between SSH slope and  $Tx$  (Figure 8a). Some of which have a  
 381 negative SSH slope relating to a positive  $Tx$  value where others show a positive SSH slope  
 382 with negative  $Tx$  value. Therefore the SSH slope does not always reflect the direction of  
 383 flow at depth, and thus the correct sign for  $Tx$ .

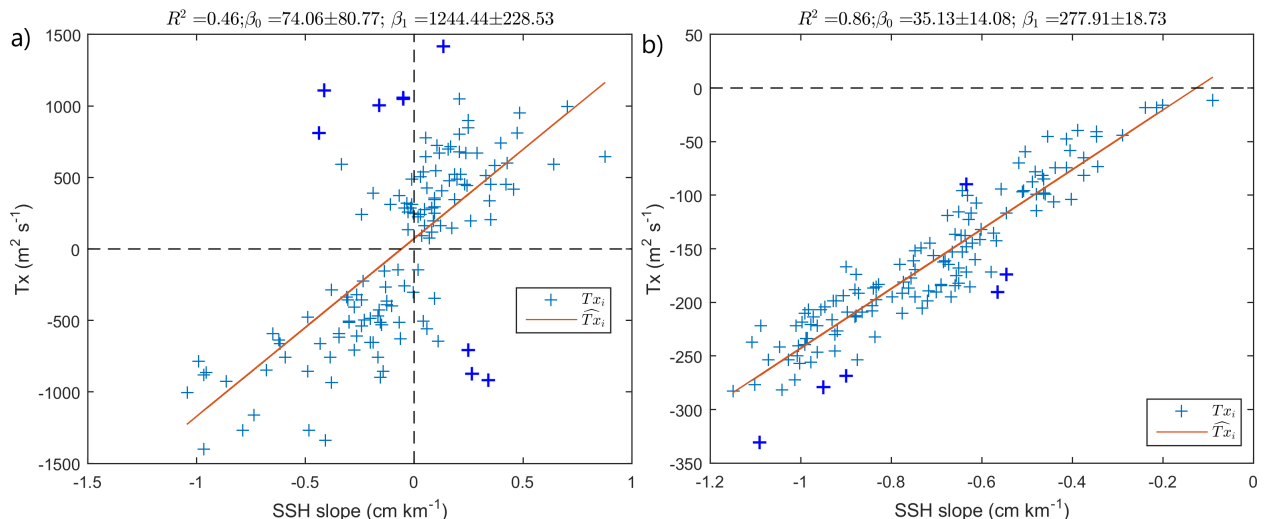


Figure 8: Linear regression models showing the relationship between HYCOM SSH and transport per unit distance ( $Tx$ ) for a) RM 8; capturing the least transport variance (46%) and b) RM 1; capturing the most transport variance (86%).  $Txi$  (blue crosses) represent the  $Tx$  values from HYCOM and  $\hat{Txi}$  (red line) represents the  $Tx$  estimates from the linear regression model. The bold crosses highlight the residual transport events with transport values greater or less than 2 standard deviations of the transport estimate. The coefficient of determination ( $R^2$ ) quantifies the amount of variance explained by the regression model,  $\beta_i$  is the slope coefficient and  $\beta_o$  the intercept with 95% confidence intervals. Note the different scaling on the x & y-axes.

384 It was expected that removing the outlying transport events (outliers larger than  $\pm 2$   
 385 standard deviations) would increase the statistical performance of the linear regression  
 386 models (Figure 4). However, it is noteworthy that the improvement was remarkably better  
 387 for the offshore regression models, since the baroclinic eddies responsible for breaking down  
 388 the linear relationship between SSH slope and transport frequently effected the offshore  
 389 edge of the current.

390 Examination of the composite cross-track velocity structure of the residual transport  
 391 events (Figure 9) shows that there is a change in the direction of velocity in the bottom  
 392 layers at the location of RM 8 (CPIES-pair P3P4). The cross-track flow in the surface  
 393 layers ( $\sim 0-700$  m) of the current is southwestward, whereas below  $\sim 700$  m the flow is  
 394 northeastward. Therefore, the vertically integrated flow ( $Tx$ ) is positive (northeastward)

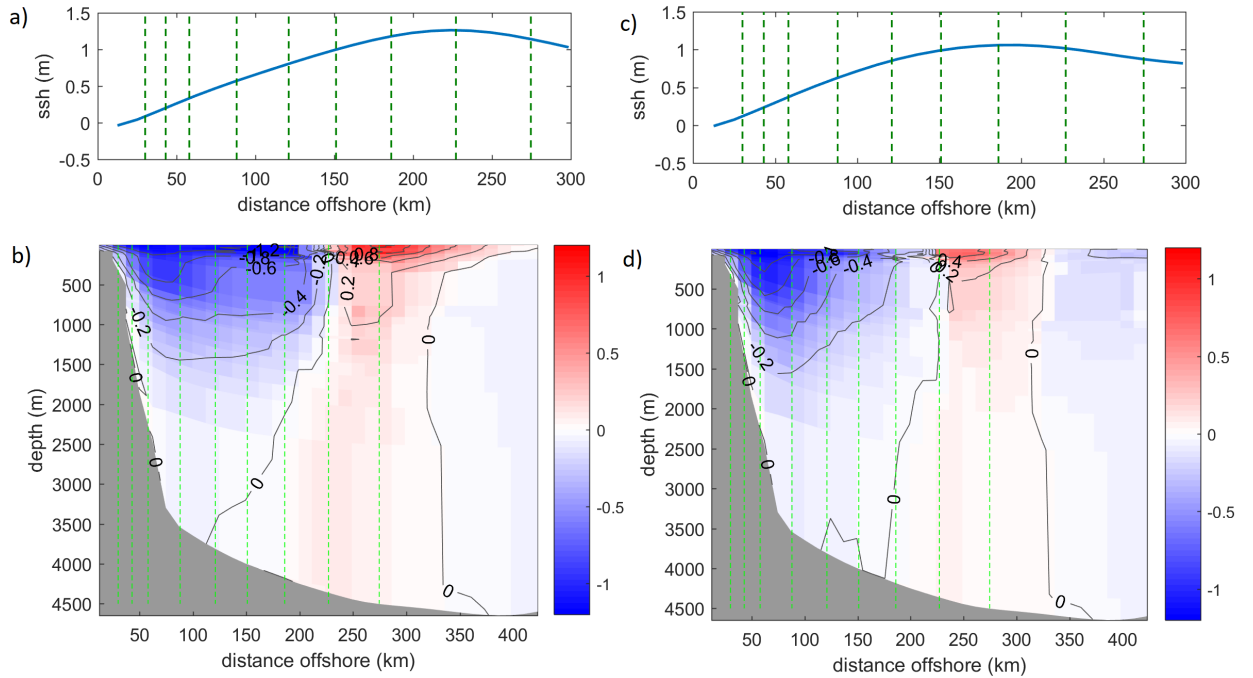


Figure 9: Mean SSH (m) and composite cross-track velocity structure ( $m s^{-1}$ ) of the residual transport events from RM 8 (a & b) and RM 1 (c & d). Blue shading represents the negative, southwest current direction and red represents the positive, northeast current flow. Contours are every  $0.2 m s^{-1}$ . Dashed vertical lines represents the nine locations of the mooring and CPIES-pairs, the first line representing mooring A and CPIES-pair P4P5 furthest offshore.

395 and in the opposite direction implied by the SSH slope. In contrast, at mooring A (RM  
 396 1), the composite velocity field is always southwestward, consistent with the SSH slope.

### 397 3.5 Sensitivity tests

398 The 34-year Agulhas transport proxy under analysis thus far was based on regression  
 399 models built using only 3 years of HYCOM model data. The statistics in Table 3 show  
 400 the results obtained from building the linear regression models and deriving the transport  
 401 proxy using 1, 3, 6, 12, 18 and 34 years of model data. We find that the correlation  
 402 between proxy box transport and model box transport is not improved by using more  
 403 years of model data to build the proxy. Using data from 2010-2013 the correlation of 0.72  
 404 changes by no more than 0.01 when extending the number of years of model data (Table  
 405 3). Similarly, building the proxy with one year of model data decreases the correlation by  
 406 only 0.01 (Table 3). The only difference was the decrease in standard deviation.

Table 3: Transport statistics and correlation results obtained from calculating the box transport proxy over a range of time periods.

Net transport	Transport (Sv)	STD (Sv)	RMSE (Sv)	r
<b>MODEL</b>	-84.32	47.23	0	1.00
<b>1-yr</b>	-87.26	35.47	33.36	0.71
<b>3-yr</b>	-87.21	34.09	32.76	0.72
<b>6-yr</b>	-87.04	35.91	33.04	0.72
<b>12-yr</b>	-86.91	32.51	32.83	0.72
<b>18-yr</b>	-88.71	31.28	32.95	0.72
<b>34-yr</b>	-88.15	29.74	33.14	0.72
<b>1980-1982</b>	-87.86	26.80	34.14	0.70
<b>2000-2002</b>	-94.80	30.31	32.87	0.72

407 The sensitivity of the box transport proxy was also tested using two arbitrary 3-year peri-  
408 ods. In comparison to the correlation obtained during 2010-2013 the correlation decreased  
409 by 0.02 during 1980-1982 and remained the same during 2000-2002. The results obtained  
410 from calculating the  $T_{box}$  proxy during the maximum (minimum) transport and standard  
411 deviation years in HYCOM showed no improvement or decrease in the skill of the proxy  
412 either.

#### 413 4 Summary and conclusions

414 The Agulhas Current transport proxies, developed by Beal and Elipot [2016], were based  
415 on nine linear regression models, each assuming a constant linear relationship from three  
416 years of observations between *in situ* transport and satellite along-track sea surface gradi-  
417 ents. Applying constant linear models and assuming a constant vertical current structure,  
418 the transport proxies were extended using 22-years of along-track satellite data to pro-  
419 duce two 22-year time-series of Agulhas Current transports [Beal and Elipot, 2016]. The  
420 Agulhas Current transport proxies in this study replicates the methods used by Beal and  
421 Elipot [2016] but applies these using a regional HYCOM model of the Agulhas Current  
422 [Backeberg et al., 2009; 2014].

423 The HYCOM transport proxies were developed using nine, three-year linear regression  
424 models between model transport and model SSH slope, and extended using 34-years  
425 of the model SSH data from 1980 to 2014. The HYCOM model provided the means to  
426 investigate the validity of the assumptions used to create the proxies, such as the constant  
427 vertical structure of the current, hence a constant relationship between SSH slope and

428 transport per unit distance during the 3-year reference period and secondly, the temporal  
429 scale of observations needed to build a strong linear relationship between transport and  
430 SSH slope.

431 Overall, results showed that the proxy was more capable of estimating the box transport  
432 (net transport) over the 34 model period, explaining 52% of the transport variance in  
433 comparison to 26% of the jet transport (southwest transport) variance. A limitation of  
434 this study is that HYCOM was unable to resolve all of the observed dynamics in the  
435 Agulhas Current, specifically the mesoscale meander events. The model demonstrated  
436 much higher levels of mesoscale variability than observed [Backeberg et al., 2008; 2009].  
437 On average, 1.6 mesoscale meanders pass through the ACT array at 34°S per year [Rouault  
438 and Penven, 2011; Elipot and Beal, 2015]. In HYCOM, an average of 5 anticyclonic eddies  
439 passed over the array per year. The poorer performance of the  $T_{jet}$  proxy in HYCOM  
440 (26%) compared to the *in situ*  $T_{jet}$  proxy (55%) of Beal and Elipot [2016] is due to various  
441 model discrepancies including the consistent merging of the anticyclonic eddies with the  
442 Agulhas Current in the northern region [Backeberg et al., 2014], which is due to poorly  
443 resolved eddy interactions and dissipation processes [Braby et al., 2016], a limitation of  
444 many numerical ocean models in this region [Tsugawa and Hasumi, 2010; Penven et al.,  
445 2011; Durgadoo et al., 2013; Backeberg et al., 2014; Loveday et al., 2014].

446 Furthermore, although the resolution of HYCOM is able to capture the mesoscale dy-  
447 namics of eddies [Holton et al., 2017], it fails to resolve the near-coastal features, such as  
448 the inshore, surface intensified cyclonic motion in this simulation. This would require a  
449 finer resolution at the coast, in order to reveal smaller offshore displacements, ~50 km,  
450 associated with these meander events [Elipot and Beal, 2015]. The poorer performance of  
451 the  $T_{jet}$  proxy in HYCOM and possibly in the *in situ* study, may also be because it only  
452 represents the southwestward component of the flow, whereas the input sea surface slope  
453 reflects the net flow along the array. Therefore, based on these findings further analysis  
454 focused on the  $T_{box}$  proxy only.

455 The frequently impinging eddies have been found to make it difficult to effectively estim-  
456 ate the accurate box transport of the Agulhas Current in the model since the advection of  
457 these eddies are responsible for large transport fluctuations [Backeberg et al., 2009]. The  
458 transport proxy only included the transport of the portion of the eddy that was reflected

459 in the SSH signal across the array, whether it was the southwestward or northeastward  
460 portion of the eddy or both. Although the transport proxy may capture the SSH signal  
461 of the eddies along the array, the correlation of the regression models decreases offshore.  
462 Therefore transport estimates inshore would be more accurate than the transport estim-  
463 ates offshore when the current is in a meandering state.

464 It was shown that removing the residual transport events, violating the proportional re-  
465 lationship between SSH slope and transport as a result of impinging baroclinic eddies,  
466 improved the proxy performance i.e. increased the percentage of transport variance ex-  
467 plained. Several studies have suggested methods to decrease the levels of EKE in numerical  
468 simulations. Backeberg et al. [2009] improved the representation of the southern Agulhas  
469 Current by applying a higher-order momentum advection scheme, resulting in a well-  
470 defined meandering current rather than a continuous stream of eddies. Anderson et al.  
471 [2011] found that the use of relative wind forcing significantly decreased eddy intensities  
472 and a study by Renault et al. [2017] focused on the current stress feedback between the  
473 ocean and atmosphere, demonstrated a reduction of mesoscale variability by coupling the  
474 ocean model with an atmospheric model. Improving the mesoscale variability in HYCOM  
475 could therefore yield better results for the transport proxy, specifically for the offshore  
476 regression models, in the future. In order to effectively mirror the performance of the *in*  
477 *situ* transport proxy [Beal and Elipot, 2016], a numerical model that accurately simulates  
478 Agulhas meanders and the vertical variability, including an accurate representation of the  
479 Agulhas Undercurrent is required and this has not yet been achieved in existing regional  
480 configurations.

481 The development of the ACT transport proxy was initially tested using a regional NEMO  
482 configuration in order to evaluate the potential of the altimeter proxy to monitor the  
483 multi-decadal transport of the Agulhas Current [van Sebille et al., 2010]. Using the  
484 numerical model, it was concluded that the correlation between the Agulhas Current  
485 transport and gradient in sea surface height was greater than  $r=0.78$  for any three-year  
486 measuring period, and is therefore an adequate timescale to build an accurate transport  
487 proxy [van Sebille et al., 2010].

488 The HYCOM output in this study was used to test the sensitivity of the relationship  
489 between transport and SSH slope over a range of time periods. It was hypothesised that



490 building the linear relationship over longer time periods, >3 years, would increase the skill  
491 of the transport proxy, since the linear relationship would include more current variability  
492 over longer periods of time. The results showed that calculating the transport proxy over  
493 longer or shorter time periods did not necessarily improve the performance of the proxy,  
494 thereby suggesting that the current dynamics for any 3-year period in the model could be  
495 very similar, in agreement with the results obtained in van Sebille et al. [2010], suggesting  
496 that the results were consistent despite the model biases. This suggests that 3-years is  
497 an appropriate time-period to develop the transport proxy of the Agulhas Current in  
498 HYCOM.

499 Lastly, the study showed that the transport proxy is sensitive to subsurface variability in  
500 the model, hence caution should be taken regarding the implicit assumption of a fixed  
501 vertical current structure. The accuracy of the transport proxy remains sensitive to model  
502 bias. Hence the sensitivity of the proxy should be tested in other model simulations.  
503 Sensitivity studies of this kind, using numerical ocean models, provide useful information  
504 advancing our understanding of the sensitivities and limitations of transport proxies,  
505 contributing to the improvement of long-term ocean monitoring approaches and assisting  
506 in the development and planning of future measurement programmes.

507 *\*Authors contributions*

508 E.V. conducted the data analyses and wrote up the final paper. B.B provided the HYCOM  
509 model data, supervised the project and provided financial support. J.H. supervised the  
510 project and provided financial support and S.E. assisted with the methodology of the  
511 transport proxy. All authors helped to conceptualize ideas and contributed to writing the  
512 paper.

513 Authors have no conflicts of interest to disclose.

514 *\*Acknowledgements*

515 This work has been funded by the National Research Foundation of South Africa and  
516 by the bilateral South Africa-Norway SANCOOP SCAMPI project. We would like to  
517 thank the Nansen-Tutu Centre in South Africa and SAEON for providing opportunities  
518 to present the project locally and internationally. We thank the Nansen Environmental  
519 Remote Sensing Centre (NERSC) in Bergen, Norway, for hosting us for a duration of  
520 the project and wish to thank Dr. Knut-Arild Lisæter for his guidance while working  
521 at NERSC. This work has also received a grant for computer time from the Norwegian  
522 Program for supercomputing (NOTUR project number nn2993k). We gratefully acknow-  
523 ledge Professor Lisa Beal, Dr. Shane Elipot and the rest of the ASCA team from the  
524 Rosenstiel School of Marine and Atmospheric Science (RSMAS), University of Miami,  
525 for granting us permission to replicate the Agulhas transport proxy methods. Shane Eli-  
526 pot was supported by the U.S. National Science Foundation through the ASCA project,  
527 Award OCE-1459543.

## 528 **References**

- 529 Anderson, L. A., McGillicuddy, D. J., Maltrud, M. E., Lima, I. D., and Doney, S. C.: Im-  
530 pact of eddy-wind interaction on eddy demographics and phytoplankton community  
531 structure in a model of the North Atlantic Ocean, *Dynamics of Atmospheres and*  
532 *Oceans*, 52, 80–94, <https://doi.org/10.1016/j.dynatmoce.2011.01.003>, 2011.
- 533 Andres, M., Park, J.-H., Wimbush, M., X-H, Z., Chang, K., and Ichikawa, H.: Study  
534 of the Kuroshio / Ryukyu Current System Based on Satellite-Altimeter and in situ  
535 Measurements, *Journal of Oceanography*, 64, 937–950, 2008.
- 536 Backeberg, B. C., Johannessen, J. A., Bertino, L., and Reason, C. J.: The greater Agulhas  
537 Current system: An integrated study of its mesoscale variability, *Journal of Physical*  
538 *Oceanography*, 1, 29–44, 2008.
- 539 Backeberg, B. C., Bertino, L., and Johannessen, J. A.: Evaluating two numerical advec-  
540 tion schemes in HYCOM for eddy-resolving modelling of the Agulhas Current, *Ocean*  
541 *Science*, pp. 173–190, 2009.
- 542 Backeberg, B. C., Penven, P., and Rouault, M.: Impact of intensified Indian Ocean winds  
543 on mesoscale variability in the Agulhas system, *Nature Climate Change*, 2, 608–612,  
544 <https://doi.org/10.1038/nclimate1587>, 2012.
- 545 Backeberg, B. C., Counillon, F., Johannessen, J. a., and Pujol, M. I.: Assimilating along-  
546 track SLA data using the EnOI in an eddy resolving model of the Agulhas system,  
547 *Ocean Dynamics*, pp. 1121–1136, <https://doi.org/10.1007/s10236-014-0717-6>, 2014.
- 548 Beal, L. M. and Elipot, S.: Broadening not strengthening of the Agulhas Current since  
549 the early 1990s, *Nature Publishing Group*, 540, 570–573, [https://doi.org/10.1038/](https://doi.org/10.1038/nature19853)  
550 [nature19853](https://doi.org/10.1038/nature19853), 2016.
- 551 Beal, L. M., De Ruijter, W. P. M., Biastoch, A., and Zahn, R.: On the role of the  
552 Agulhas system in ocean circulation and climate., *Nature*, 472, 429–36, [https://doi.org/](https://doi.org/10.1038/nature09983)  
553 [10.1038/nature09983](https://doi.org/10.1038/nature09983), 2011.
- 554 Beal, L. M., Elipot, S., Houk, A., and Leber, G. M.: Capturing the Transport Variability  
555 of a Western Boundary Jet: Results from the Agulhas Current Time-Series Experiment

556 (ACT)\*, *Journal of Physical Oceanography*, 45, 1302–1324, <https://doi.org/10.1175/>  
557 JPO-D-14-0119.1, 2015.

558 Biastoch, A. and Krauss, W.: The Role of Mesoscale Eddies in the Source Regions of the  
559 Agulhas Current, *Journal of Physical Oceanography*, 29, 2303–2317, 1999.

560 Birol, F., Fuller, N., Lyard, F., Cancet, M., Nino, F., Delebecque, C., Fleury, S., Toubanc,  
561 F., Melet, A., Saraceno, M., et al.: Coastal applications from nadir altimetry: Example  
562 of the X-TRACK regional products, *Advances in Space Research*, 59, 936–953, 2017.

563 Bleck, R.: An oceanic general circulation model framed in hybrid isopycnic-Cartesian  
564 coordinates, 37, 55–88, 2002.

565 Braby, L., Backeberg, B. C., Ansorge, I., Roberts, M. J., Krug, M., and Reason, C. J. C.:  
566 Observed eddy dissipation in the Agulhas Current, *Geophysical Research Letters*, 43,  
567 8143–8150, <https://doi.org/10.1002/2016GL069480>, 2016.

568 Cai, W.: Antarctic ozone depletion causes an intensification of the Southern Ocean  
569 super-gyre circulation, *Geophysical Research Letters*, 33, 1–4, <https://doi.org/10.1029/>  
570 2005GL024911, 2006.

571 Chassignet, E. P., Hurlburt, H. E., Martin, O., Halliwell, G. R., Hogan, P. J., Wallcraft,  
572 A. J., Baraille, R., and Bleck, R.: The HYCOM (HYbrid Coordinate Ocean Model) data  
573 assimilative system, 65, 60–83, <https://doi.org/10.1016/j.jmarsys.2005.09.016>, 2007.

574 Chelton, D. B., DeSzoeke, R. A., Schlax, M. G., El Naggar, K., and Siwertz, N.: Geograph-  
575 ical Variability of the First Baroclinic Rossby Radius of Deformation, *Journal of Phys-*  
576 *ical Oceanography*, 28, 433–460, [https://doi.org/10.1175/1520-0485\(1998\)028<0433:](https://doi.org/10.1175/1520-0485(1998)028<0433:)  
577 [GVOTFB>2.0.CO;2](https://doi.org/10.1175/1520-0485(1998)028<0433:GVOTFB>2.0.CO;2), 1998.

578 de Ruijter, W. P. M., van Leeuwen, P. J., and Lutjeharms, J. R. E.: Generation and  
579 Evolution of Natal Pulses: Solitary Meanders in the Agulhas Current, *Journal of Phys-*  
580 *ical Oceanography*, 29, 3043–3055, [https://doi.org/10.1175/1520-0485\(1999\)029<3043:](https://doi.org/10.1175/1520-0485(1999)029<3043:)  
581 [GAEONP>2.0.CO;2](https://doi.org/10.1175/1520-0485(1999)029<3043:GAEONP>2.0.CO;2), 1999.

582 Dee, D. P., Uppala, S. M., Simmons, A. J., Berrisford, P., Poli, P., Kobayashi, S., Andrae,  
583 U., Balmaseda, M. A., Balsamo, G., Bauer, P., Bechtold, P., Beljaars, A. C. M., Berg,

584 L. V. D., Bidlot, J., Bormann, N., Delsol, C., Dragani, R., Fuentes, M., Geer, A. J.,  
585 and Dee, D. P.: The ERA-Interim reanalysis : configuration and performance of the  
586 data assimilation system, pp. 553–597, <https://doi.org/10.1002/qj.828>, 2011.

587 Dijkstra and de Ruijter, W.: On the Physics of the Agulhas Current : Steady Retroflection  
588 Regimes, *Journal of Physical Oceanography*, 31, 2971–2985, 2001.

589 Durgadoo, J., Loveday, B., Reason, C., Penven, P., and Biastoch, A.: Agulhas Leakage  
590 Predominantly Responds to the Southern Hemisphere Westerlies, *Journal of Physical*  
591 *Oceanography*, 43, 2113–2131, <https://doi.org/10.1175/JPO-D-13-047.1>, 2013.

592 Elipot, S. and Beal, L.: Characteristics , Energetics , and Origins of Agulhas Current  
593 Meanders and their Limited Influence on Ring Shedding, *Journal of Physical Oceanog-*  
594 *raphy*, 45, 2294—2314, 2015.

595 Fu, L.-L., Chelton, D., Le Traon, P.-Y., and Morrow, R.: Eddy Dynamics From Satellite  
596 Altimetry, *Oceanography*, 23, 14–25, <https://doi.org/10.5670/oceanog.2010.02>, 2010.

597 George, M. S., Bertino, L., O.M, J., and A, S.: Validation of a hybrid coordinate  
598 ocean model for the Indian Ocean, *Journal of Operational Oceanography*, 3, 25–38,  
599 <https://doi.org/10.1080/1755876X.2010.11020115>, 2010.

600 Gordon, A. L.: Oceanography: The brawniest retroflection, *Nature*, 421, 904–905,  
601 <https://doi.org/10.1038/421904a>, 2003.

602 Gordon, A. L., Lutjeharms, J. R., and Gründlingh, M. L.: Stratification and circulation at  
603 the Agulhas Retroflection, *Deep Sea Research Part A. Oceanographic Research Papers*,  
604 34, 565–599, [https://doi.org/10.1016/0198-0149\(87\)90006-9](https://doi.org/10.1016/0198-0149(87)90006-9), 1987.

605 Hermes, J. C., Reason, C., and Lutjeharms, J.: Modeling the Variability of the Greater  
606 Agulhas Current System, *Journal of climate*, 20, 3131–3146, <https://doi.org/10.1175/JCLI4154.1>, 2007.

608 Holton, L., Deshayes, J., Backeberg, B., Loveday, B., Hermes, J., and Reason, C.: Spatio-  
609 temporal characteristics of Agulhas leakage: a model inter-comparison study, *Climate*  
610 *dynamics*, 48, 2107–2121, 2017.

611 Imawaki, S., Uchida, H., Ichikawa, H., and Fukasawa, M.: Satellite altimeter monitoring  
612 the Kuroshio transport south of Japan, *Geophysical Research Letters*, 28, 17–20, 2001.

613 Loveday, B. R., Durgadoo, J. V., Reason, C. J., Biastoch, A., and Penven, P.: Decoupling  
614 of the Agulhas leakage from the Agulhas Current, *Journal of Physical Oceanography*,  
615 44, 1776–1797, <https://doi.org/10.1175/JPO-D-13-093.1>, 2014.

616 Lutjeharms, J. R. E.: *The Agulhas Current*, 2006.

617 Maul, G. A., Mayer, D. A., and Bushnell, M.: Statistical relationships between local sea  
618 level and weather with Florida-Bahamas cable and Pegasus measurements of Florida  
619 Current volume transport, *Journal of Geophysical Research*, 95, 3287–3296, 1990.

620 Penven, P., Herbette, S., and Rouault, M.: Ocean Modelling in the Agulhas Current  
621 System, in: *Nansen-Tutu Conference Proceedings*, pp. 17–21, [https://doi.org/10.1017/  
622 CBO9781107415324.004](https://doi.org/10.1017/CBO9781107415324.004), 2011.

623 Reason, C. J. C.: Subtropical Indian Ocean SST dipole events and southern African  
624 rainfall, *Geophysical Research Letters*, 28, 2225–2227, 2001.

625 Renault, L., McWilliams, J. C., Penven, P., Renault, L., McWilliams, J. C., and Pen-  
626 ven, P.: Modulation of the Agulhas Current Retroflexion and Leakage by Oceanic  
627 Current Interaction with the Atmosphere in Coupled Simulations, *Journal of Physical  
628 Oceanography*, 47, 2077–2100, <https://doi.org/10.1175/JPO-D-16-0168.1>, 2017.

629 Rouault, M. and Lutjeharms, J.: Estimation of sea-surface temperature around southern  
630 Africa from satellite-derived microwave observations., *South African journal of science*,  
631 99, 489–493, 2003.

632 Rouault, M., White, S. A., Reason, C. J. C., Lutjeharms, J. R. E., and Jobard, I.:  
633 Ocean Atmospheric Interaction in the Agulhas Current Region and a South African  
634 Extreme Weather Event, *Weather and Forecasting*, 17, 655–669, [https://doi.org/10.  
635 1175/1520-0434\(2002\)017<0655:OAIITA>2.0.CO;2](https://doi.org/10.1175/1520-0434(2002)017<0655:OAIITA>2.0.CO;2), 2002.

636 Rouault, M. J. and Penven, P.: New perspectives on Natal Pulses from satellite ob-  
637 servations, *Journal of Geophysical Research: Oceans*, 116, 1–14, [https://doi.org/  
638 10.1029/2010JC006866](https://doi.org/10.1029/2010JC006866), 2011.

639 Rouault, M. J., Mouche, A., Collard, F., Johannessen, J. A., and Chapron, B.: Mapping  
640 the Agulhas Current from space : An assessment of ASAR surface current velocities,  
641 Journal of Geophysical Research, 115, 1–14, <https://doi.org/10.1029/2009JC006050>,  
642 2010.

643 Smith, L., , Boudra, D., and R, B.: A Wind-Driven Isopycnic Coordinate Model of the  
644 North and Equatorial Atlantic Ocean 2 . The Atlantic Basin Experiments, Journal of  
645 Geophysical Research, 95, 105–128, 1990.

646 Sprintall, J. and Revelard, A.: The Indonesian Throughflow response to Indo-Pacific  
647 climate varaibility, Journal of Geophysical Research: Oceans, 119, 1161–1175,  
648 <https://doi.org/10.1002/2013JC009533>.Received, 2014.

649 Tsugawa, M. and Hasumi, H.: Generation and Growth Mechanism of the Natal  
650 Pulse, Journal of Physical Oceanography, 40, 1597–1612, [https://doi.org/10.1175/](https://doi.org/10.1175/2010JPO4347.1)  
651 2010JPO4347.1, 2010.

652 Uppala, S. M., Kallberg, P. W., Simmons, A. J., Andrae, U., Bechtold, V. D. C., Fiorino,  
653 M., Gibson, J. K., Haseler, J., Hernandez, A., Kelly, G. A., Li, X., Onogi, K., Saarinen,  
654 S., Sokka, N., Allan, R. P., Andersson, E., Arpe, K., Balmaseda, M. A., Beljaars, A.  
655 C. M., Berg, L. V. D., Bidlot, J., Bormann, N., Caires, S., Chevallier, F., Dethof,  
656 A., Dragosavac, M., Fisher, M., Fuentes, M., Hagemann, S., Holm, E., Hoskins, B. J.,  
657 Isaksen, L., Janssen, P. A. E. M., Jenne, R., Mcnally, A. P., Mahfouf, J., Morcrette,  
658 J., Rayner, N. A., Saunders, R. W., Simon, P., Sterl, A., Trenberth, K. E., Untch, A.,  
659 Vasiljevic, D., Viterbo, P., and Woollen, J.: The ERA-40 re-analysis, Quarterly Journal  
660 of the Royal Meteorological Society, 131, 2961–3012, <https://doi.org/10.1256/qj.04.176>,  
661 2005.

662 van Sebille, E., Beal, L. M., and Biastoch, A.: Sea surface slope as a proxy for  
663 Agulhas Current strength, Geophysical Research Letters, 37, 2–5, [https://doi.org/](https://doi.org/10.1029/2010GL042847)  
664 10.1029/2010GL042847, 2010.

665 Yan, X. M. and Sun, C.: An altimetric transport index for Kuroshio inflow northeast  
666 of Taiwan Island, Science China Earth Sciences, 58, 697–706, [https://doi.org/10.1007/](https://doi.org/10.1007/s11430-014-5024-z)  
667 s11430-014-5024-z, 2015.

- 668 Yang, H., Lohmann, G., Wei, W., Dima, M., Ionita, M., and Liu, J.: Intensification  
669 and poleward shift of subtropical western boundary currents in a warming climate,  
670 Journal of Geophysical Research: Oceans, 121, 4928–4945, [https://doi.org/10.1002/](https://doi.org/10.1002/2015JC010796)  
671 2015JC010796, 2016.
- 672 Zhu, X. H., Ichikawa, H., Ichikawa, K., and Takeuchi, K.: Volume transport variability  
673 southeast of Okinawa Island estimated from satellite altimeter data, Journal of Ocean-  
674 ography, 60, 953–962, <https://doi.org/10.1007/s10872-005-0004-8>, 2004.